D0 Note 6317
FERMILAB – TM – 2529 – E

The D0 Run IIb Luminosity Measurement

B.C.K. Casey,[2] M. Corcoran,[7] K. DeVaughan,[5] Y. Enari,[1] E. Gallas*,[2] I. Katsanos,[5] J. Linnemann,[4] J. Orduna,[7] R. Partridge†,[6] M. Prewitt,[7] H. Schellman,[3] G.R. Snow,[5] and M. Verzocchi[2]

[1] *LPNHE, Universités Paris VI and VII, CNRS/IN2P3, Paris, France*
[2] *Fermi National Accelerator Laboratory, Batavia, Illinois 60510, USA*
[3] *Northwestern University, Evanston, Illinois 60208, USA*
[4] *Michigan State University, East Lansing, Michigan 48824, USA*
[5] *University of Nebraska, Lincoln, Nebraska 68588, USA*
[6] *Brown University, Providence, Rhode Island 02912, USA*
[7] *Rice University, Houston, Texas 77005, USA*

(Dated: March 21, 2012)

An assessment of the recorded integrated luminosity is presented for data collected with the D0 detector at the Fermilab Tevatron Collider from June 2006 to September 2011 (Run IIb). In addition, a measurement of the effective cross section for inelastic interactions, also referred to as the luminosity constant, is reported. This measurement incorporates new features that lead to a substantial improvement in the precision of the result. A luminosity constant of $\sigma_{LM} = 48.3 \pm 1.9 \pm 0.6$ mb is obtained, where the first uncertainty is due to the accuracy of the inelastic cross section used by both CDF and D0, and the second uncertainty is due to D0 sources. The recorded luminosity for the highest E_T jet trigger is $\mathcal{L}_{\rm rec} = 9.2 \pm 0.4$ fb^{-1}, with a relative uncertainty of 4.3%.

PACS numbers: 13.85.Lg

I. INTRODUCTION

An essential ingredient in cross section measurements is the integrated luminosity, $\mathcal{L}$, used to normalize the data sample. At D0, the instantaneous luminosity, L, is derived from hit rates produced from inelastic proton – antiproton collisions registered in a dedicated detector system. Measured hit rates are converted to luminosity using a normalization procedure based on the total inelastic cross section, and the geometric acceptance and efficiency of the dedicated detector system for registering inelastic events. The measurement of the effective cross section for inelastic interactions, and the assessed recorded integrated luminosity for data collected with the D0 detector at the Fermilab Tevatron Collider from June 2006 to September 2011 are reported. Luminosity L varied during that period in the range (5 – 420) μb^{-1}s^{-1} (equivalent to (5 – 420)$\cdot 10^{30}$ cm^{-2}s^{-1}).

In this note, a short description of the detector used for the instantaneous luminosity measurement and of the data samples used for this study is followed by a review of the luminosity measurement technique. The following sections describe the backgrounds that affect the luminosity measurement, the calculation of the detector acceptance, and the calculation of the luminosity constant and its uncertainty. In the Appendices, the luminosity measurement technique and the background removal are described in more detail.

A. Luminosity Monitor Detector

The Luminosity Monitor (LM) [1, 2] consists of two arrays of scintillation counters mounted on the D0 endcap calorimeter cryostats as indicated in Fig. 1. In the description of the D0 detector a right-handed coordinate system is used. The z-axis is along the proton beam direction. The angles ϕ and θ are the azimuthal and polar angles, respectively. The r coordinate denotes the perpendicular distance from the z axis.

From the perspective of the proton beam, the upstream LM array is called the "north" LM and the downstream array is called the "south" LM. Each array has 24 wedge-shaped scintillation counters with fine-mesh photomultiplier tube (PMT) readout. The PMT signals are amplified on the detector and are carried on low-loss cables to the LM VME electronics where the charge and the timing of PMT signals are measured. Coverage is provided over the pseudorapidity interval of $2.7 < |\eta| < 4.4$, where $\eta = -\ln[\tan(\theta/2)]$.

The LM electronics identify in-time hits that are within ± 6.4 ns of the nominal time-of-flight from the center of the D0 detector to the LM. This window is about three times the width of the time distribution for in-time hits. Halo particles typically produce hits that are $\sim$9 ns early in one of the detectors. A luminosity coincidence is identified when there is at least one in-time hit in both the

*now at Department of Physics, Oxford University, Oxford, United Kingdom
†Visitor from SLAC National Accelerator Laboratory, Menlo Park, CA, USA

by Fermi Research Alliance, LLC under Contract No. De-AC02-07CH11359 with the United States Department of Energy.

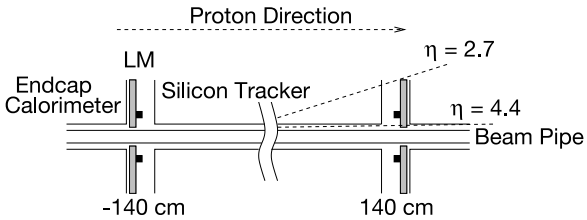

(a) $r - z$ view of the two arrays

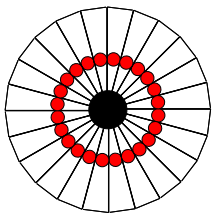

(b) $r - \phi$ view of one array

FIG. 1: The Luminosity Monitor layout. In (b) the solid dots represent the location of the PMTs.

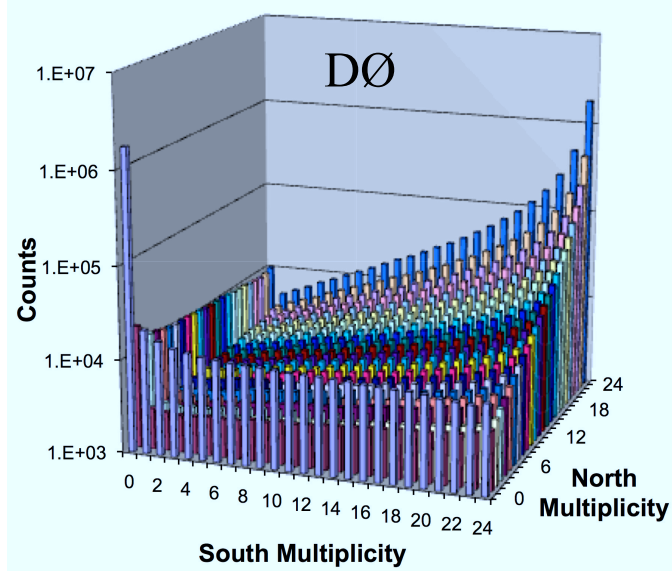

FIG. 2: 2D multiplicity distribution, after background subtraction, collected with the histogramming feature of the LM electronics.

north and the south LM detector arrays. Since beam crossings with many early hits from beam halo interactions can lead to luminosity measurement errors, a "halo veto" is applied when there are six or more early hits in one or both detector arrays. The beam crossings that do not trigger the halo veto are called "live crossings"[1].

B. Data Samples

The data sample that D0 recorded during Run II of the Fermilab Tevatron Collider is split in two periods: (i) data collected between April 2002 and February 2006 (Run IIa), and (ii) data collected from June 2006 to September 2011 (Run IIb). A major difference between the two periods is the addition of an inner silicon layer [3] to the D0 Silicon Microstrip Tracker [4] (SMT) during the 2006 shutdown. Other differences between the two periods include removal of a forward silicon disk on each end of the SMT and introduction of a new beryllium beam pipe with a flange near the LM. The readout system of the LM detector was upgraded between Runs IIa and IIb to reduce the electronic noise [5].

The data from the LM detector information includes measurements of the arrival time and pulse height information for each of the 48 LM counters. In addition, the LM electronics allow the accumulation of histograms of quantities calculated by the LM electronics for calibration and monitoring purposes. These histograms are accumulated at the beam crossing rate with no deadtime.

The Fermilab Tevatron Collider has 1113 possible radio frequency (RF) buckets. The minimal spacing between RF buckets where particles can be placed is one "tick" and corresponds to a gap of 132 ns. One turn of the Tevatron consists of 159 ticks, 36 of which generally contain beam. The ticks that actually contain particles are called "beam bunches", and the collision of proton and antiproton bunches is called a "beam crossing" or "bunch crossing". The beam bunches are arranged in 3 evenly spaced "bunch trains", separated by a 2.5 μs abort gap, and within each bunch train there are 12 beam bunches, each separated by 396 ns. Ticks that do not contain beam are referred to as "empty ticks".

The LM electronics can accumulate two-dimensional (2D) distributions of the multiplicity of in-time hits for the north and south LM detectors. An example distribution, after background subtraction, accumulated at a luminosity of 63 $\mu\mathrm{b}^{-1}\mathrm{s}^{-1}$ is shown in Fig. 2. Three distinct components can be identified: (i) empty crossings with no LM hits, (ii) single-sided interactions where only one side has hits, and (iii) double-sided interactions where both sides have hits.

In this study extensive use is made of these 2D multiplicity distributions since they increase the number of events available for study by three orders of magnitude compared to an earlier analysis [6] (Run IIa) and provide the ability to measure the multiplicity distributions for a single bunch crossing, instead of averaging over 36 bunch crossings. Consequently, rigorous background subtraction techniques can be applied. In addition, data are now acquired over a short period of time ($\sim$8 mins total) to minimize the change in luminosity while the sample is acquired. For contrast, the Run IIa analysis includes $\sim 1\%$ statistical errors due to the measurement being based in

[1] The definition of live crossings in this context is with respect to the luminosity measurement and not the D0 trigger system.

low statistics data samples (on the order of ~ 10000 beam crossings).

Histogram data samples were acquired over a period ranging from August 2008 to January 2009 for a variety of luminosities. In total, 35 such datasets were used for this study.

II. THE D0 LUMINOSITY MEASUREMENT

The D0 luminosity measurement is performed by counting the rate of north-south coincidences in the LM detectors using

$$L = \frac{1}{\sigma_{LM}} \frac{dN}{dt}, \tag{1}$$

where σ_{LM} is the effective inelastic cross section seen by the LM, referred to as the "luminosity constant". The effective inelastic cross section is derived from the total inelastic cross section, σ_{inel}, and adjusted for the LM system geometric acceptance and the efficiency for registering inelastic events. The inelastic cross section has been measured at the Tevatron by the E710, E811, and CDF experiments [7]. These experiments measure forward elastic scattering rates and use the optical theorem to determine the elastic, inelastic, and total $p\bar{p}$ cross section. A common averaging procedure [8] for the E811 and CDF measurements has been adopted by the CDF and D0 experiments, which yields an inelastic cross section of $\sigma_{inel} = 60.7 \pm 2.4$ mb at $\sqrt{s} = 1.96$ TeV.

The inelastic cross section can be subdivided into non-diffractive (σ_{nd}), single diffractive (σ_{sd}), and double diffractive (σ_{dd}) components. Single diffractive collisions are characterized by having the proton (antiproton) diffractively disassociate into hadrons while the antiproton (proton) remains intact. As in elastic collisions, the momentum transfer is typically small, so that the intact antiproton (proton) exits the detector through the beam pipe. Double diffractive collisions are similar to the single diffractive collisions except that both the proton and the antiproton undergo diffractive disassociation. Like single diffractive collisions, the particles produced tend to travel along the beam direction, thus producing large pseudorapidity gaps in the central region. Non-diffractive collisions represent the rest of the inelastic cross section and populate the full pseudorapidity region. Thus, the inelastic cross section can be expressed as

$$\sigma_{inel} = \sigma_{nd} + \sigma_{sd} + \sigma_{dd}. \tag{2}$$

The effective inelastic cross section, σ_{LM}, can be written as

$$\begin{aligned}\sigma_{LM} = \sigma_{inel}[&f_{nd}A_{nd} + (1-f_{nd})\, f_{sd}A_{sd} \\ &+ (1-f_{nd})\,(1-f_{sd})\, A_{dd}],\end{aligned} \tag{3}$$

where f_{nd} is the fraction of the inelastic cross section attributed to the non-diffractive process and f_{sd} is the fraction of the diffractive cross section attributed to the single diffractive process, given by

$$f_{nd} = \frac{\sigma_{nd}}{\sigma_{inel}}, \tag{4}$$

$$f_{sd} = \frac{\sigma_{sd}}{\sigma_{sd} + \sigma_{dd}}. \tag{5}$$

The acceptances A_{nd}, A_{sd}, and A_{dd} are the non-diffractive, single diffractive, and double diffractive acceptances, respectively, for producing at least one hit in both the north and south LM detectors.

A single-sided effective cross section σ_N (σ_S) can be defined for producing hits in only the north (south) LM detector

$$\begin{aligned}\sigma_N = \sigma_{inel}[&f_{nd}A^N_{nd} + (1-f_{nd})\, f_{sd}A^N_{sd} \\ &+ (1-f_{nd})\,(1-f_{sd})\, A^N_{dd}],\end{aligned} \tag{6}$$

$$\begin{aligned}\sigma_S = \sigma_{inel}[&f_{nd}A^S_{nd} + (1-f_{nd})\, f_{sd}A^S_{sd} \\ &+ (1-f_{nd})\,(1-f_{sd})\, A^S_{dd}],\end{aligned} \tag{7}$$

where $A^{N(S)}_{nd}$, $A^{N(S)}_{sd}$, $A^{N(S)}_{dd}$ are the non-diffractive, single diffractive, and double diffractive acceptances, respectively, for producing at least one hit in the north (south) LM detector and no hits in the south (north) LM detector. Earlier analyses of the luminosity constant [6] treated the north and south single-sided effective cross sections as being equal. In this analysis, small differences are found in both data and Monte Carlo (MC) simulations. These differences are attributed to asymmetries of the D0 detector (e.g., the north endcap calorimeter is ~ 4 cm closer to the $p\bar{p}$ interaction point than the south endcap calorimeter). Consequently, a separate calculation of the north and south single-sided acceptances and cross sections is performed.

Poisson statistics is used to determine the probability that a beam crossing will not have a north–south coincidence. This requires that there are no double-sided interactions characterized by σ_{LM}. In addition, there should be no pile-up of single-sided interactions that give hits on both the north and south sides stemming from multiple $p\bar{p}$ interactions in one beam crossing. Thus to contribute to the single-sided effective cross section, if there is a single-sided interaction on one side, there must be no single-sided interaction on the opposite side.

The probability that a beam crossing has no north-south coincidences, $P(0)$, is given by

$$\begin{aligned}&P(0) = \\ &e^{-\sigma_{LM}L/f}\left(e^{-\sigma_N L/f} + e^{-\sigma_S L/f} - e^{-(\sigma_N+\sigma_S)L/f}\right),\end{aligned} \tag{8}$$

where L is the luminosity and f is the beam crossing frequency. The first factor is the probability for having no $p\bar{p}$ interactions giving a north-south coincidence. The term in the parenthesis corrects for two single-sided interactions in the same beam crossing mimicking a north–south coincidence.

The rate of live crossings with in-time hits in both the north and south LM detectors, R_{LM}, and the live crossing rate, R_{Live}, are measured in data. The probability for an empty beam crossing is derived from these rates to be

$$P(0) = 1 - \frac{R_{LM}}{R_{Live}}. \tag{9}$$

Given $P(0)$, Eq. 8 is solved for the luminosity L, making use of the effective cross section σ_{LM} and the single-sided cross sections σ_N and σ_S. This calculation is performed for each of the 36 beam bunches independently since the luminosity, and thus $P(0)$, is different for each bunch.

This method is referred to as the "counting zeroes" technique. More details about this technique and its reach at high luminosity are presented in Appendix A.

III. LUMINOSITY MONITOR BACKGROUNDS

The LM is sensitive to two types of backgrounds: (i) out-of-time, and (ii) beam halo backgrounds. The out-of-time background is characterized by hits with an approximately uniform arrival time distribution for the ∼40 ns measurement window before the beam crossing, with a significant variation in background rate over the 12 beam bunches in a bunch train. These hits randomly occur within the LM timing window, giving rise to in-time background hits. Studies of the out-of-time background have shown (see Appendix B) that the rate of these background hits is proportional to the D0 luminosity, indicating that they are due to secondary particles from beam-beam interactions in previous beam crossings. This background is found to have an effective single-sided cross section of 0.9 ± 0.1 mb for both the north and south sides. It is assumed to originate mainly from low energy neutrons that interact in the LM scintillator, but it is possible that other sources, such as short-lived activation products, contribute.

Beam halo backgrounds occur when a proton or antiproton leaves the beam pipe upstream of the interaction point and produces secondary particles that are detected by the LM. Beam halo typically produces a shower in the upstream calorimeter that hits the upstream LM, and continues to the downstream LM. Typically, the upstream LM counters will have out-of-time hits that arrive ∼9 ns earlier than particles from beam-beam collisions, while the downstream counters will have in-time hits that arrive at approximately the same time as particles from beam-beam collisions. Beam crossings with six or more early hits are vetoed in the luminosity calculation causing ∼1% of the beam crossings to be removed. The luminosity calculation is not sensitive to the selection of the veto value.

During normal operation, the beam halo backgrounds are a few percent of the out-of-time background (e.g. for a luminosity of 100 $\mu b^{-1}s^{-1}$ with a background cross section of 0.9 mb there is a 90 kHz background rate, whereas the typical halo rates are in the range of a few kHz) and have a negligible effect on the luminosity measurement. The remainder of this section focuses on describing and removing the out-of-time background.

TABLE I: Background multiplicity rates distribution measured in an empty tick immediately before a beam crossing. The data were acquired at a luminosity of 272 $\mu b^{-1}s^{-1}$. The rows indicate the north multiplicity rate and the columns the south multiplicity rate, where the rates shown are normalized to the total number of events (5756304 events).

N/S	0	1	2	3	≥ 4
0	79%	8.1%	1.3%	0.18%	0.06%
1	9%	0.9%	0.15%	0.022%	0.007%
2	1.5%	0.18%	0.027%	0.004%	0.0011%
3	0.20%	0.023%	0.005%	0.0006%	0.0003%
≥ 4	0.06%	0.007%	0.0014%	0.0004%	0.0002%

Table I shows a typical high luminosity background rates distribution measured in an empty tick immediately before a beam crossing. One or more background hits is present in 21% of these empty ticks, and 1.3% of them have hits in both north and south LM detectors.

The largest contribution of the background in the determination of σ_{LM} occurs when an empty crossing is converted into a single-sided crossing with one background hit. Previous determinations of the σ_{LM} for Run IIa [6] have used two techniques for removing the background contribution to the hit multiplicity distribution. The first technique used sidebands in the arrival time distribution to estimate the out-of-time background in events with a single hit in the detector and make the appropriate subtraction. The second technique required at least two hits (instead of one) on the opposite side when determining the non-diffractive fraction.

For this study a different technique is used, for which a detailed description can be found in Appendix C. If signal and background hits are uncorrelated, the probability D_{ij} of having i north counters and j south counters with observed hits is given by

$$D_{ij} = \sum_{\substack{l=0\\m=0}}^{\substack{l\leq i\\m\leq j}} \sum_{\substack{p=0\\q=0}}^{\substack{p\leq i\\q\leq j}} S_{lm} B_{pq} f_{lpi} f_{mqj} \Theta(l+p-i)\,\Theta(m+q-j)\,, \tag{10}$$

where S_{lm} is the probability for having l north counters and m south counters with signal hits, B_{pq} is the probability for having p north counters and q south counters with background hits, and Θ is the Heaviside step function

$$\Theta(l+p-i) = \begin{cases} 1 & \text{for } l+p \geq i \\ 0 & \text{for } l+p < i. \end{cases} \tag{11}$$

The combinatoric factor f_{lpi} (and similarly f_{mqj}) represents the probability for observing i north counters with

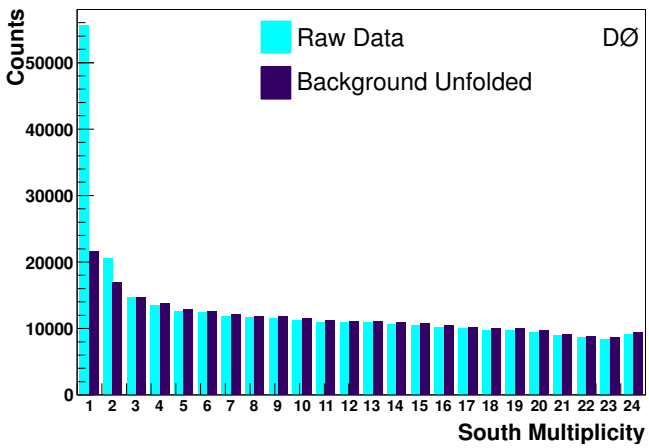

FIG. 3: Example of the effect of background subtraction. The south multiplicity distribution is plotted for beam crossings where there are no hits in the north LM detector. The "Raw Data" histogram shows the multiplicity distribution before background subtraction.

hits given that there were l north counters with signal hits and p north counters with background hits. The factor f_{lpi} is given by

$$f_{lpi} = \frac{l!\,(N-l)!p!\,(N-p)!}{(l+p-i)!\,(i-p)!\,(i-l)!\,(N-i)!N!}, \qquad (12)$$

where $N = 24$ is the number of counters on a side.

The observed signal and background probability distribution can be obtained from the multiplicity histogram associated with a beam crossing, and the background probability distribution can be obtained from the multiplicity histogram obtained from the empty tick immediately before the beam crossing. Thus, we can solve the above set of linear equations for the background-free signal probability distribution.

The effect of this background unfolding procedure is best illustrated by looking at its effect on beam crossings where one side has no hits. Figure 3 shows a slice of a 2D multiplicity distribution taken at a luminosity of 63 $\mu\mathrm{b}^{-1}\mathrm{s}^{-1}$. The slice plotted shows the south multiplicity when there are no hits in the north LM detector. The prominent peak for a single south hit is substantially reduced, as is expected from previous studies of the arrival time distribution for this bin.

The background unfolding is performed on the 2D multiplicity distribution, and it has certain features that do not appear in a 1D unfolding procedure. For example, in Fig. 3 the number of entries in the higher multiplicity bins is larger after the background unfolding procedure than for the raw data. In the 1D unfolding procedure, entries can only migrate from higher multiplicity to lower multiplicity. In a 2D unfolding procedure, entries can also migrate between 1D slices. In the example shown in Fig. 3, diffractive events with no north signal hits but > 0 north background hits are not included in the raw data (since the slice with no observed north hits is examined), but are included in the background subtracted measurement since these events truly have no north signal hits. The net effect of these two migrations is that bins with more than 3 south hits have more entries after background subtraction than before.

IV. LUMINOSITY CONSTANT DETERMINATION

A. Luminosity Monitor Acceptance Calculation

The LM acceptances are calculated by simulating non-diffractive, single diffractive, and double diffractive events in the D0 detector. Events are generated using PYTHIA [9], with the CTEQ6L1 [10] parametrization of the parton distribution functions (PDFs), and utilizing the "Tune A" parameter set [11] that is optimized to reproduce CDF data. The longitudinal distribution of the $p\bar{p}$ interaction vertex is generated as a Gaussian with an RMS of ~ 25 cm. In the transverse directions the beam is generated as a Gaussian centered at the origin with a width of about 100 μm. These Monte Carlo events are then processed through the standard D0 detector simulation based on GEANT3 [12], using a modified detector geometry with the material model adjusted to match the multiplicity distribution in the LM as observed in the data.

The number of hits that satisfy the timing criteria and have charge above threshold is counted separately for the north and south LM detectors, with the MC charge threshold and timing resolution adjusted to reproduce the data. Events are then classified into one of the following geometrical categories: (i) events that have at least one hit in both the north and south LM detectors (NS), (ii) events that have at least one hit in the north detector and no hits in the south detector (N Only), (iii) events that have at least one hit in the south detector and no hits in the north detector (S Only) and (iv) events that have no hits in either detector (Empty). The fraction of events in each category determines the associated acceptance shown in Table II. The "N Only" and "S Only" acceptances are not identical since the D0 detector, and its MC description, is not north/south symmetric.

B. Determination of the Non-Diffractive Fraction

The non-diffractive fraction can be related to the "zero fraction" measured in the data by using Poisson statistics. "Zero fraction" is the fraction of beam crossings that have no hits on a given side (north or south) when there is at least one hit on the opposite side.

Starting with the north zero fraction, the probability of having no two-sided interactions and no one-sided in-

TABLE II: LM acceptances and their statistical uncertainties, for each type of inelastic process and geometrical category.

Category	Non-Diffractive Acceptance	Single Diffractive Acceptance	Double Diffractive Acceptance
NS	0.9924 ± 0.0009	0.326 ± 0.005	0.500 ± 0.005
N Only	0.0048 ± 0.0007	0.224 ± 0.004	0.203 ± 0.004
S Only	0.0026 ± 0.0005	0.225 ± 0.004	0.212 ± 0.004
Empty	0.0002 ± 0.0001	0.225 ± 0.004	0.0857 ± 0.0028

teractions hitting the north side is

$$P\left(N=0\right)=e^{-(\sigma_{LM}+\sigma_N)L/f}. \tag{13}$$

Having zero hits on the north side while having at least one hit on the south side has a probability

$$P\left(N=0,S>0\right)=e^{-(\sigma_{LM}+\sigma_N)L/f}\left(1-e^{-\sigma_S L/f}\right). \tag{14}$$

Thus the north zero fraction is given by:

$$\begin{aligned} f_0^N &= \frac{P\left(N=0,S>0\right)}{P\left(S>0\right)} = \frac{P\left(N=0,S>0\right)}{1-P\left(S=0\right)} \\ &= \frac{e^{-(\sigma_{LM}+\sigma_N)L/f}\left(1-e^{-\sigma_S L/f}\right)}{1-e^{-(\sigma_{LM}+\sigma_S)L/f}}. \end{aligned} \tag{15}$$

The south zero fraction is obtained similarly, by exchanging σ_N with σ_S.

The cross sections in the above equations depend on the total inelastic cross section σ_{inel}, the non diffractive fraction f_{nd}, the single diffractive fraction f_{sd}, and the LM acceptances (see Eqs. 3, 6, 7). The single diffractive fraction is taken to be $f_{sd} = 0.57 \pm 0.21$ [13].

Having already evaluated the LM acceptances, the only quantity still needed is the luminosity for the data sample. In a given sample, the luminosity can be determined from the measured LM coincidence probability

$$P\left(N>0,S>0\right)=1-P\left(0\right), \tag{16}$$

where $P(0)$ is given by Eq. 8. Equations 15 and 16 are used to solve for the two remaining unknowns: the non diffractive fraction f_{nd}, and the luminosity L.

In the histogram data sample considered, 35 multiplicity histograms are acquired for the first beam bunch in the first beam train. For each of these histograms, the north and south zero fractions are calculated and the non-diffractive fraction determined. Results can be seen in Fig. 4, where the luminosity of the first beam bunch of the first beam train is extrapolated to the total delivered luminosity assuming that each beam bunch has the same luminosity. The statistical error on the non-diffractive fraction measurement ranges from 0.0006 to 0.0019 and is negligible.

The north and south non-diffractive fractions are similar but exhibit some systematic differences. The north non-diffractive fraction has a higher dispersion, and exhibits a small correlation with luminosity which is attributed to the effects of beam halo, where the rate for

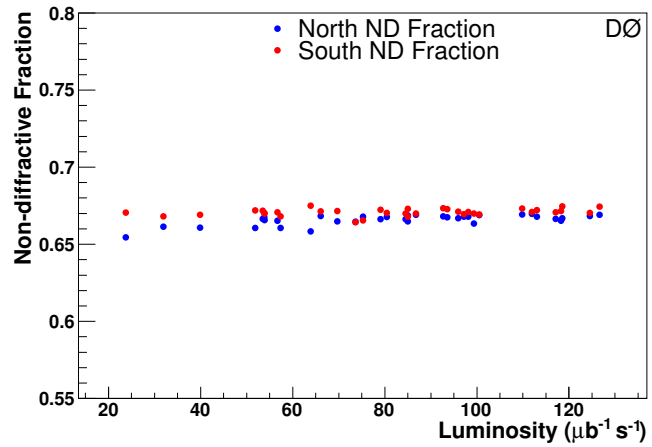

FIG. 4: Non-diffractive fraction measurements as a function of luminosity. Separate fits are performed to the north and south zero fractions.

proton halo is in most cases substantially larger than for antiproton halo. Proton halo creates out-of-time hits in the north LM detector and in-time hits in the south LM detector. If a proton beam halo event occurs during an otherwise empty crossing, it will be counted as a single-sided event, thus increasing the north zero fraction. Since the diffractive processes are much more likely to have single-sided events than the non-diffractive processes, an increased zero fraction corresponds to a decrease in the non-diffractive fraction. The fraction of empty beam crossings decreases rapidly with increasing luminosity, so that the effect of beam halo is largest at low luminosity, which is consistent with the observed trend. The observed north/south difference is considered as a systematic uncertainty in the calculation of σ_{LM}. Averaging the north and the south non-diffractive fractions for the 35 luminosity points considered results in $\langle f_{nd}\rangle = 0.668$ with an RMS spread of 0.002.

C. Luminosity Constant

The calculated LM acceptances (Table II) and the non-diffractive fraction (evaluated in section IV B), together with $\sigma_{inel} = 60.7 \pm 2.4$ mb and $f_{sd} = 0.57 \pm 0.21$ are used to determine the luminosity constant, σ_{LM}, based on Eq. 3, for each data sample. Figure 5 shows the consis-

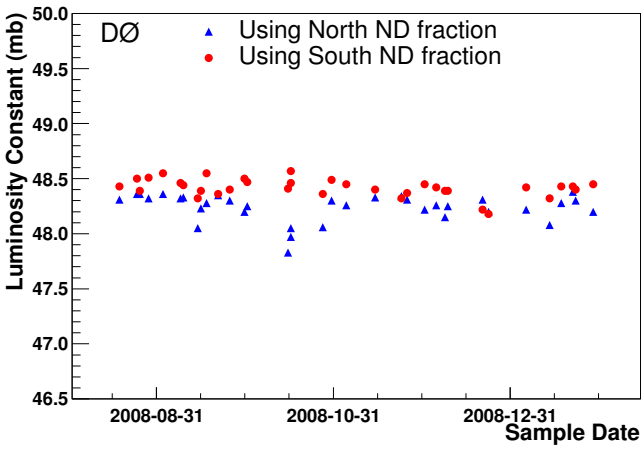

FIG. 5: Measured luminosity constant as a function of time.

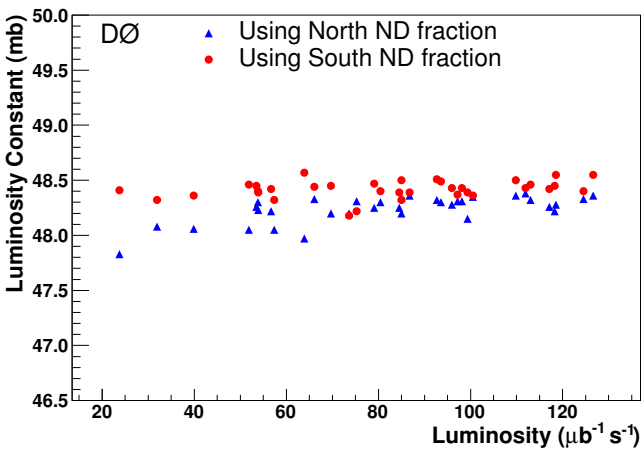

FIG. 6: Measured luminosity constant as a function of the D0 luminosity.

tency of the measurement of σ_{LM} during the period of ≈6 months when the multiplicity histograms were collected. The luminosity constant is labeled as "North" when the north non-diffractive fraction has been used, while it is labeled as "South" when the south non-diffractive fraction has been used. Figure 6 shows the luminosity dependence of the σ_{LM} determination, which indicates a similar trend to the one observed for the non-diffractive fraction (see Fig. 4). The statistical uncertainty on the σ_{LM} measurements ranges from 0.02 to 0.07 mb.

The distribution of the σ_{LM} measurements is shown in Fig. 7. The average of the north and south luminosity constants gives

$$\sigma_{LM} = 48.3 \text{ mb}. \tag{17}$$

The north and south single sided cross sections are determined to be

$$\sigma_N = \sigma_S = 4.5 \text{ mb}. \tag{18}$$

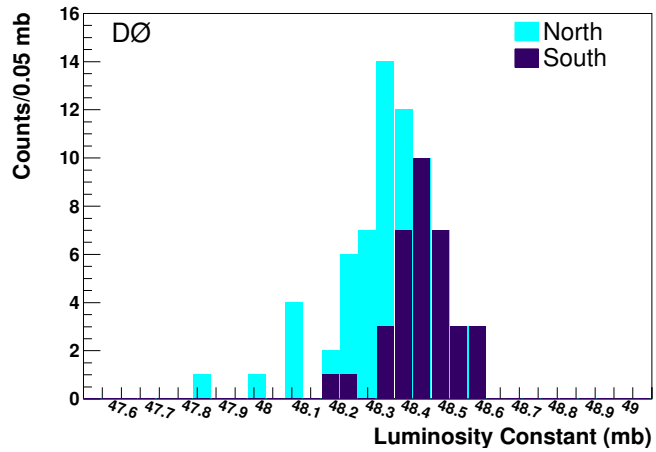

FIG. 7: Distribution of luminosity constant measurements.

D. Luminosity Constant Uncertainty

In evaluating the systematic uncertainties affecting the measurement of σ_{LM}, the different sources are propagated through the analysis chain to establish the effect on σ_{LM}, including re-calculating the LM acceptances and determining the non-diffractive fraction for each data sample. This allows us to take into account the correlation between the LM acceptances and the non-diffractive fraction. The different sources of systematic uncertainties are listed below:

Inelastic Cross Section

The CDF and D0 experiments have adopted [8] an inelastic cross section of $\sigma_{inel} = 60.7 \pm 2.4$ mb at $\sqrt{s} = 1.96$ TeV for their luminosity measurements. Propagating the 2.4 mb uncertainty in the inelastic cross section gives an uncertainty of 1.91 mb on the luminosity constant, σ_{LM}.

Single Diffractive Fraction

The single diffractive fraction is taken to be $f_{sd} = 0.57 \pm 0.21$ [13], corresponding to a large variation in the single diffractive cross section. This corresponds to an uncertainty of 0.43 mb on σ_{LM}.

Time Variation / Radiation Damage

Periodic adjustments to the PMT high voltage are performed, and the LM scintillators are replaced during long shutdowns to minimize the impact of radiation damage. The high voltage changes typically lead to less than 0.5% change in the measured luminosity. An uncertainty of ±0.5% (0.24 mb) is assigned to σ_{LM} due to time variation in the luminosity measurement.

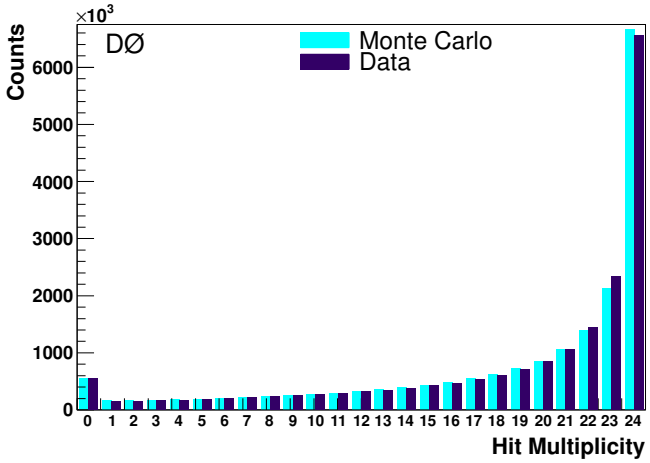

FIG. 8: Hit multiplicity when there are one or more hits on the opposite side. The north and south distributions have been combined to reduce MC statistical errors. The data are from a background subtracted multiplicity histogram taken at a luminosity of 63 $\mu b^{-1}s^{-1}$. The MC samples represent the tuned material model.

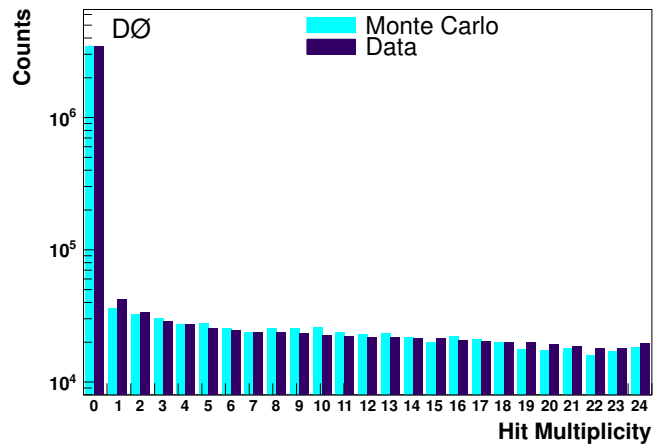

FIG. 9: Hit multiplicity when there are no hits on the opposite side. The north and south distributions have been combined to reduce MC statistical errors. The data are from a background subtracted multiplicity histogram taken at a luminosity of 63 $\mu b^{-1}s^{-1}$. The MC samples represent the tuned material model.

GEANT Energy Cutoffs

The simulated events are reprocessed through the D0 GEANT3 [12] simulation with lower energy cutoffs. The δ ray production cutoff is lowered from 1 MeV to 10 keV, the neutral and charged hadron cutoffs are lowered from 1 MeV to 100 keV, and the muon cutoff is lowered from 10 MeV to 100 keV. The 100 keV energy cutoff selected for this study is based on an estimate of the lowest energy that could cause an LM counter to detect a hit. A change of 0.24 mb in σ_{LM} is observed, and this is assigned as a systematic uncertainty.

Monte Carlo Material Model

In order to have the MC reproduce the observed hit multiplicity distribution, it is necessary to modify the material in front of the LM in the GEANT3 model. MC events have been generated both with the nominal (untuned) material model and the tuned material model. The resulting change in σ_{LM} of 0.16 mb is taken as a systematic uncertainty.

As a check that the tuned material model reproduces the hit multiplicity histograms, Figs. 8 and 9 show the hit multiplicity for a histogram acquired at a luminosity of 63 $\mu b^{-1}s^{-1}$. The data points have the out-of-time background contribution removed using the background unfolding procedure described in Appendix C. In Fig. 8 at least one opposite side hit is required, while in Fig. 9 the requirement is that there are no opposite side hits. The hit multiplicity distributions for these data and MC samples are observed to be in good agreement.

Luminosity Monitor Acceptance

The acceptance of the LM shows a small dependence (less than 0.1%) due to the longitudinal variation in the location of the $p\bar{p}$ interaction vertex. In addition, the variations in the transverse position of the interactions[2] results in a 0.17% variation in the LM acceptance. Adding these effects in quadrature with the Monte Carlo statistics yields an uncertainty of 0.11 mb on σ_{LM}.

Light Collection / Radiation Damage

Radiation damage can reduce the light collection efficiency [14]. To estimate this contribution, MC events with a piece-wise linear change in the light collection efficiency were generated. The light collection efficiency is reduced by a factor of two at the inner edges of the scintillator wedge, increasing linearly to no change at the center of the PMT, and then decreasing linearly to a factor of two reduction at the outer edge of the wedge. The charge threshold is also adjusted to emulate the effect of the HV changes that work to keep

[2] The beam position could vary as much as 0.3 mm around the nominal transverse location during normal data taking, and the nominal transverse location was 1.6 mm off center before October 2007 and was moved to 0.2 mm off center for stores after that time.

the average charge constant. These changes in the MC efficiency calculation resulted in a change in σ_{LM} of 0.09 mb, which is assigned as a systematic uncertainty.

North – South Asymmetry

The north and south σ_{LM} measurements differ by an average of 0.18 mb. Since the final value of σ_{LM} is selected to be the average of the north and south measurements, a systematic uncertainty of 0.09 mb is assigned to σ_{LM} to account for the observed north – south asymmetry.

Luminosity Dependence

In the ensemble of 35 σ_{LM} measurements made at varying luminosities, an RMS spread of 0.08 mb is observed, so this value is assigned as a systematic to account for the observed luminosity dependence.

PDF Choice

The standard D0 PDF set is CTEQ6L1 [10]. Events were also generated using MRST2004NLO [15]. This change resulted in a difference of 0.06 mb in σ_{LM}, which is assigned as an uncertainty.

PYTHIA Tune

Events have been generated with a modified value for the transition point between the low-p_{T} and high-p_{T} models, as an alternative to modifying the material model. This is done by changing the PYTHIA [9] parameter PARP(82), which is known to have a significant affect on the average multiplicity, from the default value of 2.0 to 1.25. This change in the PYTHIA parameter led to a change in σ_{LM} of 0.04 mb, which is assigned as a systematic uncertainty.

Background Unfolding

The σ_{LM} calculation is repeated using multiplicity histograms acquired during the last bunch crossing of a bunch train. These bunches have ≈40% higher background than the first bunch of a bunch train. The difference of 0.03 mb between the two calculations is assigned as a systematic uncertainty associated with the background unfolding.

GEANT Hadronic Model

For this study, the GCalor [16] hadronic model is replaced with the Geisha [17] model due to its ability to better handle low energy particle interactions. This change in the GEANT hadronic model resulted in a 0.03 mb change in σ_{LM}, which is assigned as a systematic uncertainty.

TABLE III: Contributions to the luminosity constant (σ_{LM}) uncertainty.

Source	Uncertainty (mb)
Inelastic Cross Section	±1.91
Single Diffractive Fraction	±0.43
Time Variation / Radiation Damage	±0.24
GEANT Energy Cutoffs	±0.24
Monte Carlo Material Model	±0.16
Luminosity Monitor Acceptance	±0.11
Light Collection / Radiation Damage	±0.09
North – South Asymmetry	±0.09
Luminosity Dependence	±0.08
PDF Choice	±0.06
Pythia Tune	±0.04
Background Unfolding	±0.03
GEANT Hadronic Model	±0.03
Seasonal Timing Variation	±0.02
Charge Threshold	±0.01

Seasonal Timing Variation

There are seasonal drifts in the D0 clock stemming from temperature variations that result in expansion or contraction of the long cable used to send signal for collisions from the accelerator control room. To account for the effect of seasonal timing observed, the timing window of ±6.4 ns that defines an in-time hit is shifted by ±1 ns. The resulting change of 0.02 mb in σ_{LM} is assigned as a systematic uncertainty.

Charge Threshold

The charge threshold in the MC simulation is shifted by ±2 pC around the nominal value of 8 pC to account for uncertainties in the modeling of the charge threshold. The resulting change of 0.01 mb in σ_{LM} is assigned as a systematic uncertainty.

The luminosity constant (σ_{LM}) uncertainties are summarized in Table III. Adding the uncertainties in quadrature yields an uncertainty in σ_{LM} of ±2.0 mb, where 1.9 mb is associated with the uncertainty in the inelastic cross section, 0.4 mb is associated with the uncertainty in the single diffractive fraction, and 0.4 mb is associated with the remaining sources of uncertainty.

V. INTEGRATED LUMINOSITY

The integrated luminosity $\mathcal{L}$, defined as

$$\mathcal{L} = \int_0^T L \cdot dt, \tag{19}$$

where T is the data taking period, is the relevant quantity used in the measurements of cross sections and in setting

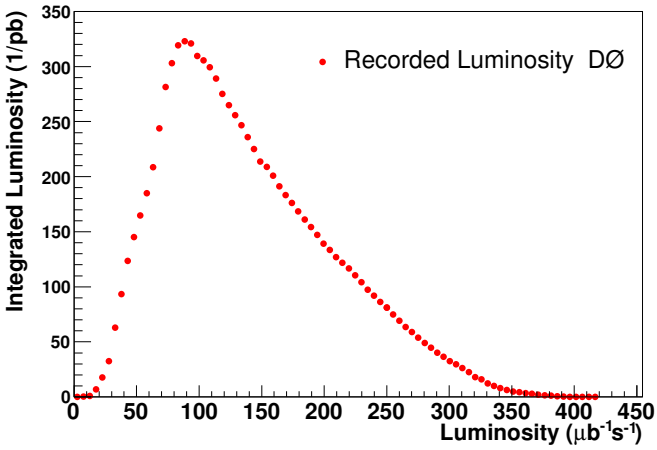

FIG. 10: The recorded luminosity profile in bins of 5 μb^{-1}s^{-1}.

upper limits on the production of new particles. In addition to the uncertainty on the luminosity constant, the uncertainty on the determination of the integrated luminosity takes into account additional contributions that cover possible variations with time and with luminosity of the luminosity constant. These additional sources of uncertainty are discussed below.

The "delivered" luminosity is the integrated luminosity delivered by the Tevatron. The "recorded" luminosity is the integrated luminosity associated with a specific trigger and takes into account the deadtime and losses in the data acquisition system. Level 1 triggers are grouped together so that they have common deadtime, i.e., common sources of enable, disable, and readout [2]. The recorded integrated luminosity referred to in this section corresponds to the luminosity exposure of the experiment's jet trigger with the highest transverse energy, $E_T = E \cdot \sin\theta$, which requires at least one jet with $E_T > 125$ GeV.

The total recorded integrated luminosity for Run IIb is assessed to be 9.2 fb^{-1}. Of that, $\sim$0.2 fb^{-1} were recorded with luminosity above 300 μb^{-1}s^{-1}, and $\sim$1.7 fb^{-1} were recorded with luminosity between 200 and 300 μb^{-1}s^{-1}. Figure 10 shows the recorded luminosity profile, in bins of width 5 μb^{-1}s^{-1}, for the full Run IIb dataset.

A. Long-Term Stability of the Luminosity Measurement

The yield of single muons in the forward muon system [18] can be used as an independent check of the stability of the luminosity measurements. The single muon yield Y is monitored regularly using special data samples and is obtained by

$$Y = \frac{N_\mu}{\mathcal{L}}, \tag{20}$$

where N_μ is the number of the forward muons, and $\mathcal{L}$ is the integrated luminosity of the respective data sample.

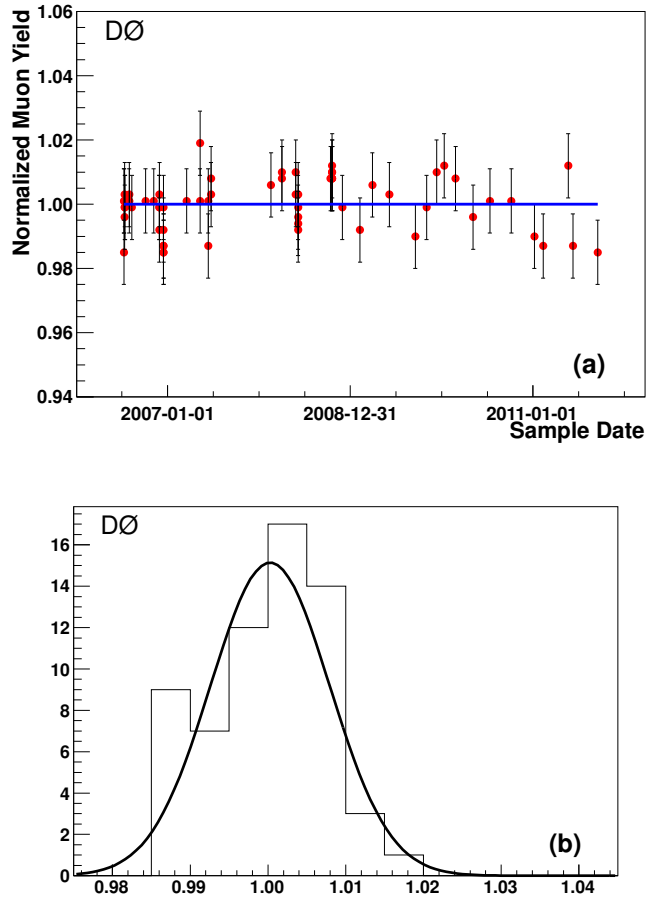

FIG. 11: Normalized single muon yields (a) as a function of time, and (b) its projection on the y-axis.

The normalized yield is obtained by dividing the value of the muon yield for each data sample by the mean value of all the data samples collected

$$Y_{\text{norm}} = \frac{Y}{\text{mean value}}. \tag{21}$$

Figure 11(a) shows the normalized yield measurements for Run IIb. If the statistical error on N_μ is less than 1% the uncertainty on the yield, σ_Y, is set to 1%; otherwise σ_Y is set to the statistical error of N_μ. Figure 11(b) shows the distribution of the normalized muon yields super-imposed with a Gaussian function that indicates a typical variation of $\sim$0.8%.

In addition, muon yields are measured as a function of luminosity. Figure 12 shows an example of the distribution of the normalized muon yields collected during two Tevatron stores. The super-imposed Gaussian on Fig. 12(b) indicates a typical variation of $\sim$0.4%. After accounting for the statistical errors on N_μ and the uncertainty due to the time variation / radiation damage already included in the luminosity constant, a systematic uncertainty of 0.6% is assigned to the integrated luminos-

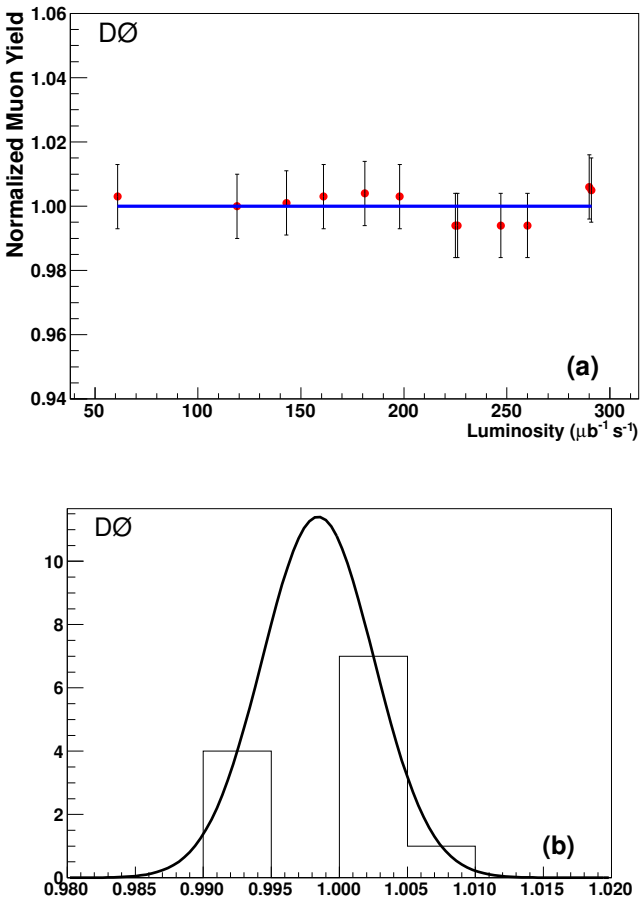

FIG. 12: Normalized single muon yields (a) as a function of luminosity, and (b) its projection on the y-axis.

ity measurement based on the observed variation in the muon yield.

B. Integrated Luminosity Measurement Uncertainty

The uncertainty of the integrated luminosity includes a dominant contribution of 4.2% stemming from the uncertainty on the luminosity constant. Additionally, it includes an uncorrelated contribution of 0.6% in the integrated luminosity measurement described in the previous section. Other potential source of systematic uncertainty includes events that are lost in the D0 data acquisition and reconstruction system and are not properly taken into account. The fraction of these events has been studied and found to be negligible ($<<$ 0.1%).

Adding these uncertainties in quadrature yields an uncertainty in the integrated luminosity of 4.3%, where 4.0% originates from the uncertainty in the inelastic cross section and is correlated with both the CDF and D0 Run IIa integrated luminosity measurements, 0.9% originates from the uncertainty in the single diffractive fraction and uncorrelated with the CDF integrated luminosity measurement, but correlated with the D0 Run IIa integrated luminosity measurement, and 1.0% originates from the remaining sources of uncertainty that are uncorrelated with both the CDF and D0 Run IIa integrated luminosity measurements.

VI. SUMMARY AND CONCLUSIONS

In summary, we have measured the effective inelastic cross section, σ_{LM}, as seen by the D0 luminosity monitor, and assessed the recorded integrated luminosity for data collected with the D0 detector at the Fermilab Tevatron Collider for the period called Run IIb (June 2006 to September 2011). A luminosity constant of $\sigma_{LM} = 48.3 \pm 2.0$ mb is obtained. The Run IIb luminosity constant is 0.6% larger than the Run IIa luminosity constant (48.0 ± 2.9 mb) and its uncertainty has been reduced from 6.1% to 4.2%.

The recorded integrated luminosity for the highest E_T jet trigger is $\mathcal{L} = 9.2 \pm 0.4$ fb^{-1} during Run IIb. The total relative uncertainty of the Run IIb D0 recorded integrated luminosity is determined to be 4.3%, where 4.0% is associated with the inelastic cross section, 0.9% is associated with the single diffractive fraction, and 1.0% is associated with the D0 sources of uncertainty.

We thank the staffs at Fermilab and collaborating institutions, and all our D0 collaborators for their support. In particular we would like to extend our gratitude to Brad Abbott of the University of Oklahoma and David Hedin of the Northern Illinois University for the thorough review of this document and their insightful comments, Margherita Vittone – Wiersma of the Fermilab Computing Division for her tireless work on the luminosity database, and Andrey Shchukin of the Institute for High Energy Physics, Protvino, Russia for providing the muon yields data and plots. We also acknowledge support from the DOE and NSF (USA); CEA and CNRS/IN2P3 (France); FASI, Rosatom and RFBR (Russia); CNPq, FAPERJ, FAPESP and FUNDUNESP (Brazil); DAE and DST (India); Colciencias (Colombia); CONACyT (Mexico); KRF and KOSEF (Korea); CONICET and UBACyT (Argentina); FOM (The Netherlands); STFC and the Royal Society (United Kingdom); MSMT and GACR (Czech Republic); CRC Program and NSERC (Canada); BMBF and DFG (Germany); SFI (Ireland); The Swedish Research Council (Sweden); and CAS and CNSF (China).

[1] C-C. Miao, FERMILAB-Conf-98/395-E (1998).

[2] D0 Collaboration, V. Abazov et al., Nucl. Instrum. Meth-

ods A 565 (2006) 463.
[3] R. Angstadt et al., Nucl. Instrum. Meth. A 622 (2010) 298.
[4] S. N. Ahmed et al., Nucl. Instrum. Meth. A 634 (2011) 8.
[5] J. Anderson et al., Nuclear Science Symposium Conference Record, IEEE 1 (2006) 503.
[6] T. Andeen et al., FERMILAB-TM-2365 (2007).
[7] N. A. Amos et al., Phys. Lett. B 301 (1993) 313;
C. Avila et al., Phys. Lett. B 445 (1999) 419;
F. Abe et al., Phys. Rev. D 50 (1994) 5550.
[8] S. Klimenko, J. Konigsberg, T. M. Liss, FERMILAB-FN-0741 (2003).
[9] T. Sjöstrand et al., Comput. Phys. Commun. 135 (2001) 238.
[10] J. Pumplin et al., J. High Energy Phys. 07 (2002) 012;
D. Stump et al., J. High Energy Phys. 10 (2003) 046.
[11] R. Field, eConf C010630 (2001) 501.
[12] R. Brun, F. Carminati, CERN Program Library Long Writeup W5013, 1993 (unpublished).
[13] T. Edwards et al., FERMILAB-TM-2278 (2004);
CDF Collaboration, F. Abe et al., Phys. Rev. D50 (1994) 5535;
CDF Collaboration, T. Affolder et al., Phys. Rev. Lett. 87 (2001) 141802.
[14] B. Casey et al., Nuclear Science Symposium Conference Record, IEEE 2 (2006) 1192.
[15] A. D. Martin et al., Phys. Lett. B604 (2004) 292.
[16] C. Zeitnitz, T. A. Gabriel, Nucl. Instr. Meth. A 349 (1994) 106.
[17] H. C. Fesefeldt, Technical Report PITHA 85–02 (1985).
[18] V. Abazov et al., Nucl. Instrum. Methods A 552 (2005) 372.

Appendix A: Empty Crossing Method

The D0 luminosity is derived from the number of beam crossings with north – south in-time coincidences in the D0 LM that occur during a measurement period. The luminosity reported to the Fermilab accelerator division for monitoring purposes is based on a nominal 15 s measurement period, while the luminosity used for physics analyses employs a nominal 60 s measurement period. The actual measurement period is occasionally shorter to ensure synchronization between the luminosity measurement and the state of the data acquisition system. Statistical fluctuations in the number of luminosity coincidences lead to statistical and systematic errors in individual luminosity measurements.

The luminosity calculation is performed separately for each of the 36 beam bunches in the Tevatron, resulting in each bunch having its own measured luminosity. For a bunch with true luminosity L, the average number of proton – antiproton interactions that produce north – south coincidences is proportional to the luminosity

$$\overline{N}_{NS}(L) = \frac{\sigma_{LM}}{f} L, \tag{A1}$$

where σ_{LM} is the effective inelastic cross section seen by the LM and f is the beam crossing frequency. Similarly, the average number of interactions in a beam crossing that produce in-time hits in only the north (south) LM array is given by

$$\begin{aligned} \overline{N}_N(L) &= \frac{\sigma_N}{f} L, \\ \overline{N}_S(L) &= \frac{\sigma_S}{f} L, \end{aligned} \tag{A2}$$

where σ_N and σ_S are the single-sided effective cross sections.

The fraction of beam crossings that do not produce a north-south coincidence of in-time LM hits are classified as empty and, using Poisson statistics, is given by

$$\begin{aligned} F_0(L) &= e^{-\overline{N}_{LM}(L)} \\ &\cdot \left(e^{-\overline{N}_N(L)} + e^{-\overline{N}_S(L)} - e^{-(\overline{N}_N(L)+\overline{N}_S(L))} \right), \end{aligned} \tag{A3}$$

where the first factor is the probability for having no $p\bar{p}$ interactions giving a north-south coincidence. The term in the parenthesis gives the probability for not having multiple single-sided interactions that result in a north-south coincidence.

The average number of empty crossings during a measurement period is then

$$\overline{N}_0(L) = N_{\text{Live}} \times F_0(L), \tag{A4}$$

where N_{Live} is the number of live beam crossings during the measurement period. In the results shown below, we ignore the small fraction of beam crossings that are rejected due to halo veto ($\sim$1%) and we consider $N_{\text{Live}} = f \cdot T$, where T is the measurement period.

1. Behavior of the D0 Luminosity Measurement at High Luminosity

The number of empty crossings observed in different measurement periods can be described with the binomial distribution. In the high luminosity limit where the number of empty crossings is small, the distribution of the observed number of empty crossings is well approximated by a Poisson distribution

$$P(n_0) = \frac{n^{\overline{N}_0(L)}}{n!} e^{-\overline{N}_0(L)}, \tag{A5}$$

where $P(n_0)$ is the probability of observing n_0 empty crossings.

For each measurement period, the measured luminosity L_m corresponding to the observed number of empty beam crossings, n_0, is calculated by numerically solving the equation

$$\begin{aligned} n_0 &= N_{Live} e^{-\sigma_{LM} L_m/f} \\ &\cdot \left(e^{-\sigma_N L_m/f} + e^{-\sigma_S L_m/f} - e^{-(\sigma_N+\sigma_S) L_m/f} \right). \end{aligned} \tag{A6}$$

In the case where no empty crossings are observed, the solution of the above equation yields an infinite measured luminosity. When that occurs, the luminosity is set to the value that would be found if there had been one empty crossing observed. The impact of this approximation on the measurement of the luminosity in D0 is discussed below.

The average measured luminosity is given by

$$\overline{L}_m = P(0)L_m(1) + \sum_{n_0=1}^{fT} P(n_0)L_m(n_0) \qquad \text{(A7)}$$

where $P(n_0)$ is the probability of observing n_0 empty crossings, and the first term accounts for the special handling where no empty crossings are observed.

The total luminosity is obtained by summing the luminosity from the 36 beam bunches. If all 36 bunches had the same luminosity, the total luminosity would be 36 times the bunch luminosity and the RMS spread of the total luminosity would be a factor of six times the RMS for a single bunch since each bunch measurement is statistically independent. In practice there are typically a few percent variations among the bunch luminosities. While these bunch-to-bunch variations are accounted for in the D0 luminosity measurement, the results following illustrate the behavior of the measured total luminosity under the assumption that all bunches have the same bunch luminosity. Including typical bunch-to-bunch variations will not significantly affect these results.

The relation between the average measured luminosity and the true luminosity for measurements periods of 15 s and 60 s is shown in Fig. 13. Due to the non-linear behavior in the empty crossing probability at high luminosity, the average measured luminosity systematically exceeds the true luminosity before entering the saturation region, where the luminosity asymptotically approaches the value $L_m(1)$ that is assigned to bunches with less than two empty beam crossings.

Table IV illustrates how the non-linear behavior of the empty crossing probability and the special treatment of the case where there are no empty crossings in the measurement period lead to non-linear behavior for the average measured luminosity. In this example, the true luminosity is 420 $\mu\text{b}^{-1}\text{s}^{-1}$, the measurement period is 15 s, and the average number of empty crossings in the measurement period is 3.05. The exponential decrease in the measured luminosity as the number of observed empty crossings increases results in an average measured luminosity of 424.8 $\mu\text{b}^{-1}\text{s}^{-1}$, which is 1.1% higher than the true luminosity.

Figure 14 shows the mean deviation between the average measured luminosity and the true luminosity as a function of the true luminosity. The largest positive deviation occurs when the average number of empty crossings is ~ 3. This occurs at a luminosity of 420 $\mu\text{b}^{-1}\text{s}^{-1}$ for a 15 s measurement period, where the average number of interactions with a north-south coincidence is ~ 12 and the fraction of empty crossings is $\sim 4 \cdot 10^{-6}$. For a 60 s measurement period, an average of 3 empty crossings occurs at a luminosity of 470 $\mu\text{b}^{-1}\text{s}^{-1}$, where the average number of interactions with a north-south coincidence is ~ 13 and the fraction of empty crossings is $\sim 10^{-6}$. Given that only a small fraction of data was collected at luminosities in excess of 300 $\mu\text{b}^{-1}\text{s}^{-1}$ and that the measurement period used for the determination of the integrated luminosity is of 60 s, we estimate that the impact of the non-linear behavior in the empty crossing probabilities has a negligible impact on the precision of the integrated luminosity determination in D0.

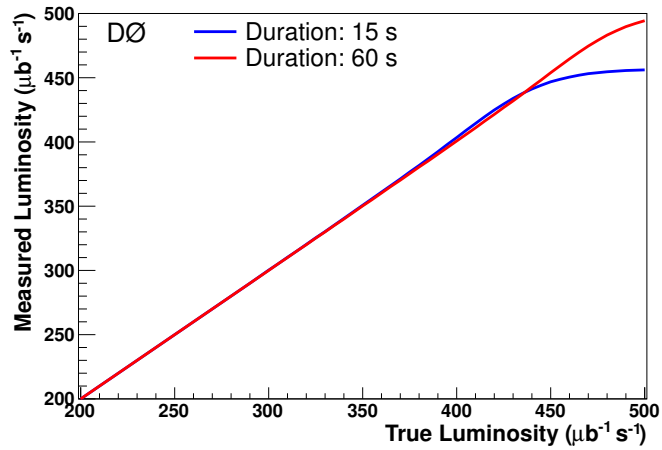

FIG. 13: Average measured luminosity versus the true luminosity for 15 s and 60 s measurement periods.

TABLE IV: Non-linearity in the luminosity measurement showing the probability, measured luminosity, and contribution to the average luminosity as a function of the observed number of empty crossings. In this example, the true luminosity is 420 $\mu\text{b}^{-1}\text{s}^{-1}$ and the measurement period is 15 s.

n_0	$P(n_0)$	L_m ($\mu\text{b}^{-1}\text{s}^{-1}$)	$P(n_0) \cdot L_m$ ($\mu\text{b}^{-1}\text{s}^{-1}$)
0	0.047	456.9	21.7
1	0.145	456.9	66.1
2	0.220	434.0	95.7
3	0.224	420.5	94.2
4	0.171	411.0	70.1
5	0.104	403.6	42.0
6	0.053	397.5	21.0
> 6	0.036	–	14.0
Sum	1	–	424.8

The RMS width of the measured luminosity for a single bunch is given by

$$\sigma^2_{L_m} = P(0)\left(L_m(1) - \overline{L}_m\right)^2 + \sum_{n_0=1}^{fT} P(n_0)\left(L_m(n_0) - \overline{L}_m\right)^2, \qquad \text{(A8)}$$

where the first term accounts for the special handling where there are no empty crossings observed. The statistical uncertainty in the total luminosity for the 36 bunches is shown in Fig. 15. The statistical uncertainty

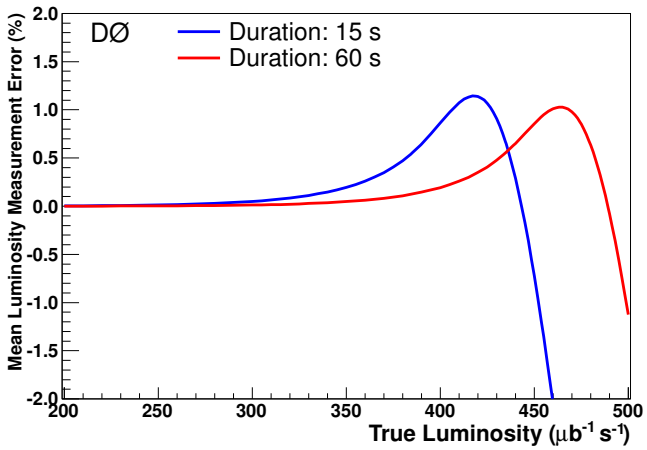

FIG. 14: Mean deviation between the average measured luminosity and the true luminosity for 15 s and 60 s measurement periods.

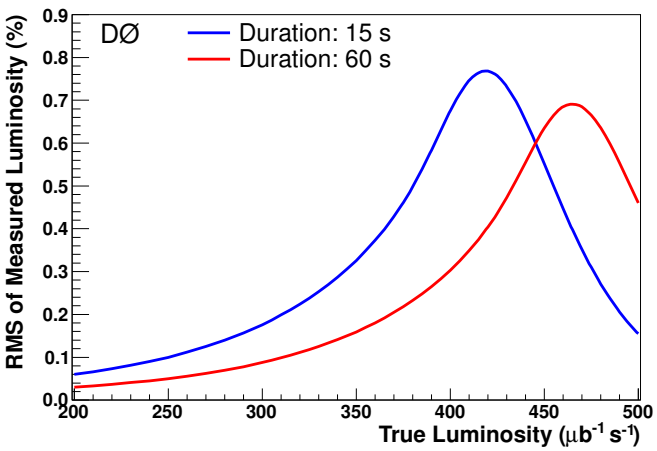

FIG. 15: RMS width of the measured luminosity for 15 s and 60 s measurement periods.

in the luminosity measurement is less than 0.1% for luminosities in the range 1.5 – 250 μb^{-1}s^{-1} for the 15 s measurement period and 0.4 – 310 μb^{-1}s^{-1} for the 60 s measurement period. The RMS width reaches a maximum of $\sim 0.7\%$ when the average number of empty crossings is ~ 3. Further increases in the true luminosity push the luminosity measurement into the saturation region where an increasing fraction of luminosity measurements report the maximum possible measured luminosity $L_m(1)$, leading to a decrease in the RMS width.

At high luminosity, the statistical error can be approximated by

$$\frac{\sigma_L}{L} \approx \frac{1}{\sqrt{N_B}} \frac{1}{\overline{N}_{NS}} \frac{\sigma_{R_0}}{R_0}, \tag{A9}$$

where R_0 is the rate of empty crossings, N_B is the number of beam bunches, and the small contribution to the empty crossing rate from multiple single-sided interactions is ignored. Thus, the large statistical error on the empty crossing rate when there are an average of 3 empty crossings ($1/\sqrt{3}$ or 58%) is reduced by a factor of six due to the 36 independent bunch measurements and an additional factor of ~ 12 at 420 μb^{-1}s^{-1} due to the exponentially falling empty crossing rate to yield a precision in the total luminosity of better than 1%.

A key requirement for the empty crossing method to work at high luminosity is that beam crossings with in-time north-south coincidences are not misclassified as empty crossings. With empty crossings rates in the part-per-million range at peak luminosities, this misclassification probability must be well under 10^{-6} for typical beam crossings. Such beam crossings are easily identified in the D0 LM since a typical beam crossing yields in-time hits in most or all of the 24 luminosity counters, whereas the requirement is ≥ 1 in-time hit. Since early hits in a large number of counters can mask the presence of in-time hits, a halo veto has been implemented to exclude beam crossings with more than six early hits from the luminosity calculation. Timing distributions are monitored and the LM TDCs are recalibrated as needed to ensure that the timing distributions are well centered within the timing window. Tests of the digital counting electronics have proven this system to be robust with no evidence of misclassification.

Appendix B: Background Studies

1. Luminosity Dependence of Background Rate

The luminosity dependence of the rate for background hits in bunch crossings that do not have proton-antiproton collisions is studied, where the multiplicity of background hits is neglected and only the fraction of beam crossings with > 0 hits in the LM is measured. The north and south background rates, and the coincidence rate where background hits occur in both north and south counters are separately measured. Figure 16(a) shows the background rates as a function of luminosity, measured in an empty tick 132 ns before the first bunch crossing of a bunch train. Figure 16(b) shows the same rates measured in an empty tick 396 ns after the last bunch crossing of a bunch train. In both cases, the north and the south rates scale approximately linearly with luminosity, while the north – south coincidence rate is much lower and has a non-linear dependence on luminosity.

2. Effective Background Cross Section

Since the north and south background rates scale linearly with the luminosity, the background rate can be treated as an effective background cross section. Since there is no actual luminosity in the ticks where the backgrounds are measured, 1/36 of the D0 luminosity (i.e.,

the average luminosity attributable to one of the 36 beam bunches) is taken to calculate the background cross section.

To account for pileup in the background, Poisson statistics is used to relate the background cross section and the background rate R_{BG} in a given detector using

$$P(0) = e^{-\sigma_{BG} L/f} = 1 - \frac{R_{BG}}{f} \tag{B1}$$

$$\sigma_{BG} = -\frac{f}{L} \ln\left(1 - \frac{R_{BG}}{f}\right), \tag{B2}$$

where σ_{BG} is the background cross section, L is the luminosity, f is the beam crossing frequency, and R_{BG} is the background rate.

Figure 17 shows that the background cross section is largely independent of the luminosity. The background cross section after a bunch train is about 40% higher than immediately before the bunch train, indicating that the background cross section increases during the bunch train.

For a given bunch crossing, the background cross section is observed to decrease over time, as shown in Fig. 18, and attributed to radiation damage to the scintillator. The cross section increases significantly in data recorded in late January 2009 immediately following an increase in the high voltage applied to the LM PMTs to compensate for the radiation damage. There is also an increase in the background rate in early October 2008, following a long downtime of the accelerator, interpreted as evidence of some annealing of the radiation damage in the scintillator following an extended shutdown. Averaging the 140 background cross section measurements from 35 data samples shown in Fig. 17, the average background cross section is estimated to be: $\sigma_{BG} = 0.85$ mb.

3. Background Characteristics

The coincidence background where both north and south luminosity monitors recorded hits is studied, since such coincidences are counted in the luminosity measurement. Table V shows a high luminosity background multiplicity distribution for an empty tick immediately before a bunch train. One or more background hits are present in 21% of the beam crossings, and 1.3% of the beam crossings have hits in both north and south luminosity monitors. The multiplicity of background hits is low. Approximately 79% of beam crossings with background hits have only one background hit among the 48 luminosity counters.

The question whether the north and south background hits are statistically independent is studied by projecting the 2D distributions to obtain 1D probability distributions for observing a particular number of hits in the north/south monitor. Table VI shows the 1D probability distributions derived from the 2D multiplicity distribution in Table V, where $P_N(i)$ is the probability of having i counters hit in the north luminosity monitor and $P_S(j)$ is the probability of having j counters hit in the south luminosity monitor.

If the backgrounds in the north and the south detectors are uncorrelated, the number of entries in the 2D

TABLE V: Background multiplicity distribution measured in an empty tick immediately before a beam crossing. The data were acquired at a luminosity of 272 $\mu b^{-1}s^{-1}$. The rows indicate the north multiplicity and the columns the south multiplicity.

N/S	0	1	2	3	≥ 4
0	4522672	466907	76071	10313	3203
1	501848	52260	8699	1265	394
2	84467	9072	1524	208	63
3	11706	1349	263	33	17
≥ 4	3460	399	78	23	10

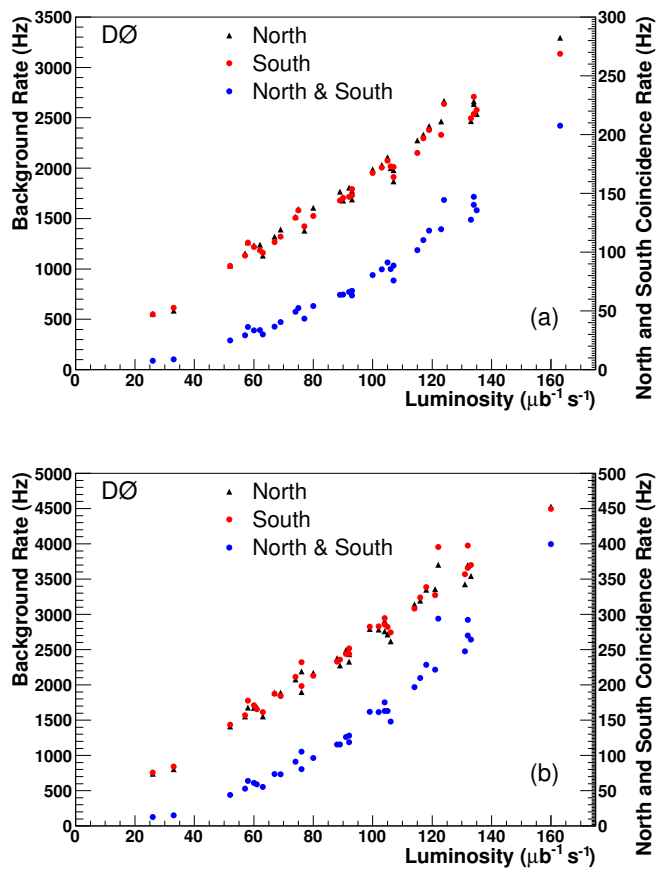

FIG. 16: Background rate, measured in an empty tick (a) immediately before the first bunch crossing and (b) 396 ns after the last bunch crossing of a bunch train. One or more background hits in the north/south luminosity monitors is required (left axis). Also shown is the rate of beam crossings in which both north and south luminosity monitors have one or more background hits (right axis).

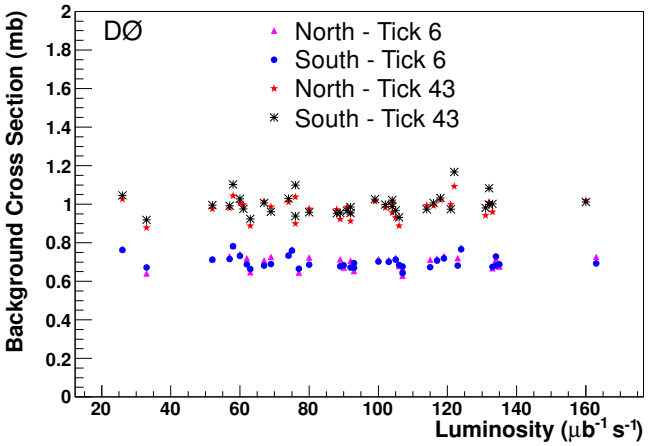

FIG. 17: Effective background cross section as a function of luminosity, measured in an empty tick 132 ns before (tick 6) and 396 ns after (tick 43) a bunch train.

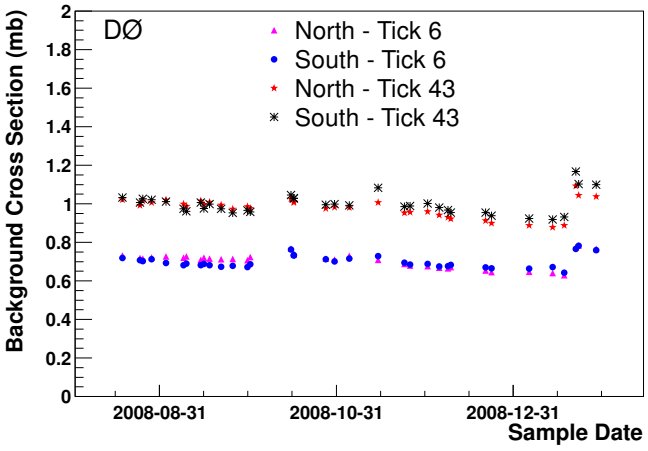

FIG. 18: Time dependence of the background cross sections. The increase in the cross section in late January 2009 corresponds to the raising of the PMT high voltages to compensate for radiation damage. The PMT high voltages were adjusted a few days before the first data point in the plot. Tick 6 refers to an empty tick immediately before a bunch train, and tick 43 refers to an empty tick after a bunch train.

multiplicity distribution, $N(i,j)$, will be given by

$$N(i,j) = P_N(i)P_S(j)N_0, \tag{B3}$$

where N_0 is the total number of entries in the 2D multiplicity distribution. Table VII shows the predicted 2D multiplicity distribution using this equation and the 1D probability distributions in Table VI. Reasonably good agreement is observed between the measured 2D multiplicity distributions shown in Table V and the predicted distribution in Table VII. Nevertheless, there is a small but persistent underestimate in the number of predicted coincidences between north and south detectors.

TABLE VI: North and south 1D probability distributions derived from the 2D multiplicity distribution in Table V.

Multiplicity	P_N	P_S
0	0.8824	0.8902
1	0.09806	0.0921
2	0.01656	0.0151
3	0.0023	0.0021
≥ 4	0.0007	0.0006

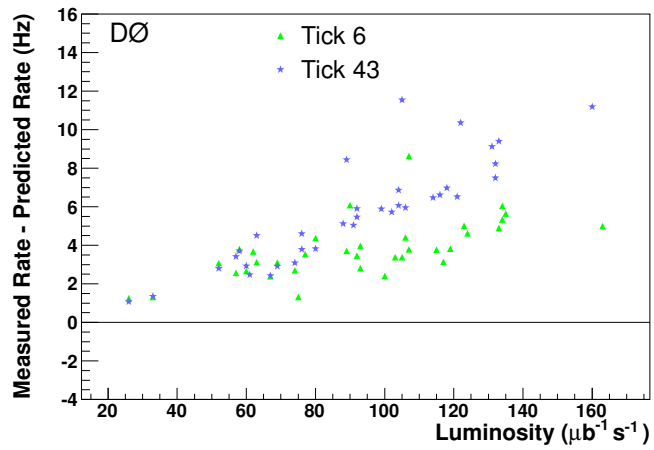

FIG. 19: Difference between the measured and predicted rates before (Tick 6) and after (Tick 43) bunch train crossings with hits in both north and south luminosity monitors.

Figure 19 shows the difference between the predicted and measured rate for observing north − south background coincidences for the data sample considered. The predicted rate is consistently underestimated by a small amount, and the magnitude of the discrepancy grows with luminosity.

There are no additional known sources of background that can give north − south coincidences. In predicting the random coincidence rate, the assumption was made that there are no correlations in the probabilities that the north and south detectors have background hits. Since the rate of background hits scales with luminosity, the background must be associated with beam − beam interactions in previous beam crossings. The number of interactions in a given beam crossing will fluctuate according to Poisson statistics. Beam crossings with upward fluctuations in the number of interactions will have a higher probability of producing background hits in both the north and south luminosity monitors, while crossings with a downward fluctuation will have a lower probability of producing background hits.

Let P represent the probability of producing a background hit in either the north or south luminosity monitor for a given beam crossing. Instead of assuming a fixed value for P, it is assumed that P fluctuates depending on how many beam − beam interactions took place in

TABLE VII: Predicted 2D probability distribution obtained from the 1D probability distributions in Table VI under the assumption that the north and south 1D distributions are statistically independent.

N/S	0	1	2	3	≥ 4
0	4521378	467642	76444	10448	3253
1	502477	51971	8495	1161	362
2	84865	8777	1434	196	61
3	11900	1231	201	27	9
≥ 4	3534	366	60	8	3

recent beam crossings. The probability of having a north – south coincidence, P_{coin}, is given by

$$\begin{aligned}\langle P_{coin}\rangle &= \langle P^2\rangle \\ &= \langle P\rangle^2 + \sigma_P^2,\end{aligned} \tag{B4}$$

where σ_P is the RMS spread of the P distribution. If there is an average of N_{eff} beam – beam interactions producing background hits, we obtain:

$$\frac{\sigma_P}{\langle P\rangle} = \frac{1}{\sqrt{N_{eff}}} \tag{B5}$$

and

$$\langle P_{coin}\rangle = \langle P\rangle^2\left(1+\frac{1}{N_{eff}}\right). \tag{B6}$$

Assuming that each of the 36 beam crossings has the same luminosity, $L = L_{tot}/36$, and that the background hits effectively arise from the previous m beam crossings, we obtain

$$N_{\rm eff} = m\frac{\sigma_{\rm LM}L}{f} \tag{B7}$$

The parameter m is estimated by fitting the data. Using empty ticks prior to a bunch train crossing gives an estimate of $m \approx 7$ and after the bunch train crossing $m \approx 9$. The difference between the predicted and measured north – south coincidence rates, both with and without correcting for fluctuations in the background probability, are shown in Fig. 20. The background model gives good agreement between the predicted and measured coincidence rate provided that the background probability is allowed to fluctuate.

4. Background during Beam Crossings

The aim is to estimate the background cross section for beam crossings, but the method discussed up to now is not applicable to actual beam crossings. A model is developed that allows the estimation of the background cross section during beam crossings. Using this model, it is found that the average background cross section for the 36 beam crossings is slightly higher than what is obtained by averaging the background cross sections before and after the beam crossing.

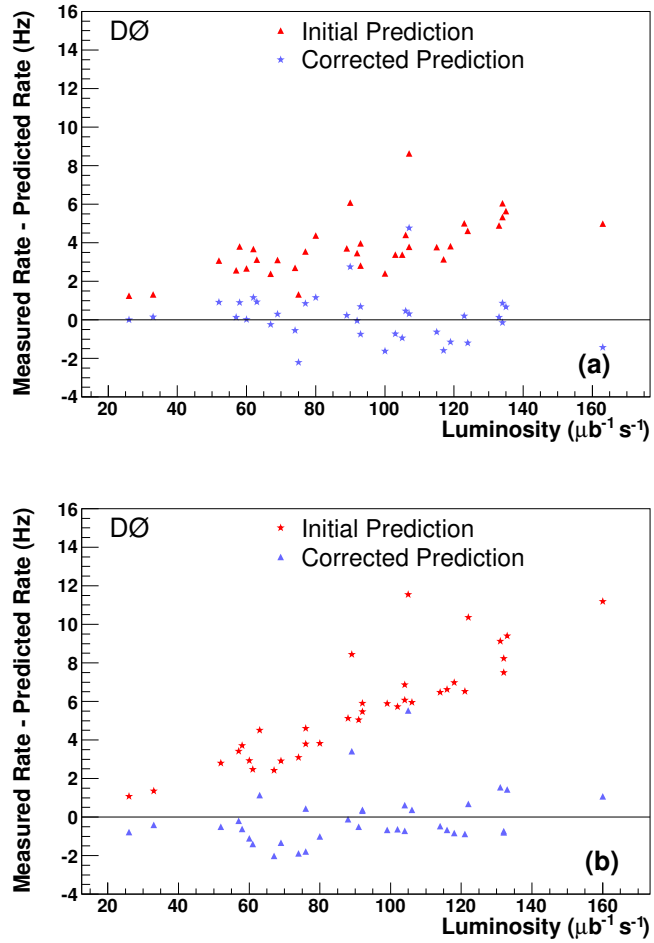

FIG. 20: Difference between the measured and predicted rates for bunch train crossings with hits in both north and south luminosity monitors (a) before and (b) after the bunch train. The prediction of Eq. B3 assumes a fixed background probability, whereas the corrected prediction allows the background probability to fluctuate.

The probability of producing a background hit in the north or south luminosity monitors is estimated from the coincidence probability

$$P = \sqrt{\frac{P_{coin}}{1+N_{eff}^{-1}}}, \tag{B8}$$

The corresponding background cross section is calculated using Poisson statistics to account for pileup

$$\sigma_{BG} = -\frac{f}{L}\ln\left(1-P\right). \tag{B9}$$

Figure 21 shows the background cross section for data recorded over the span of one minute on November 12,

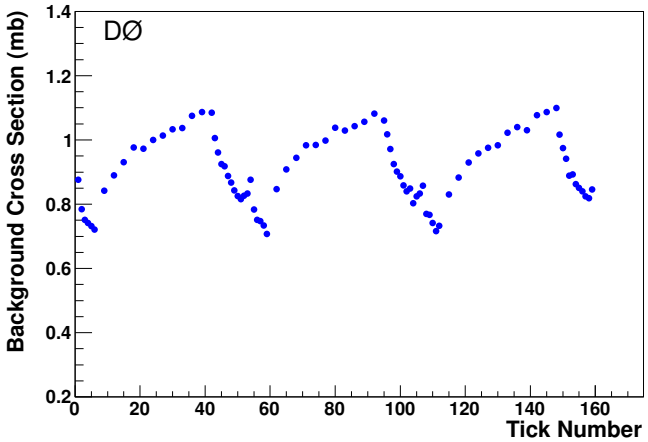

FIG. 21: Background cross section during bunch crossings.

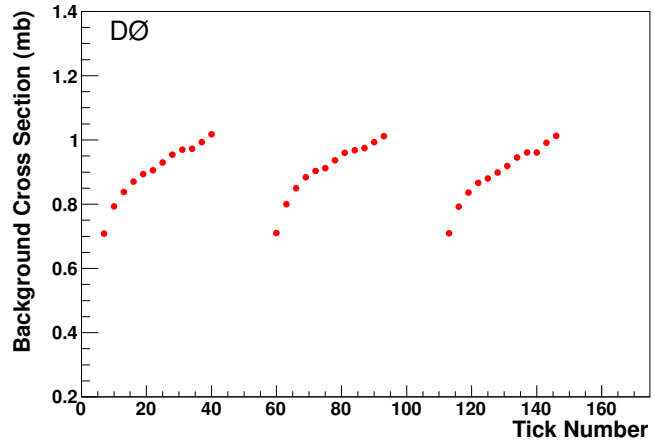

FIG. 23: Predicted background cross section.

2008 at a luminosity of 68 $\mu\mathrm{b}^{-1}\mathrm{s}^{-1}$. The background cross section rises during the course of bunch crossings and then decays in the region without bunch crossings.

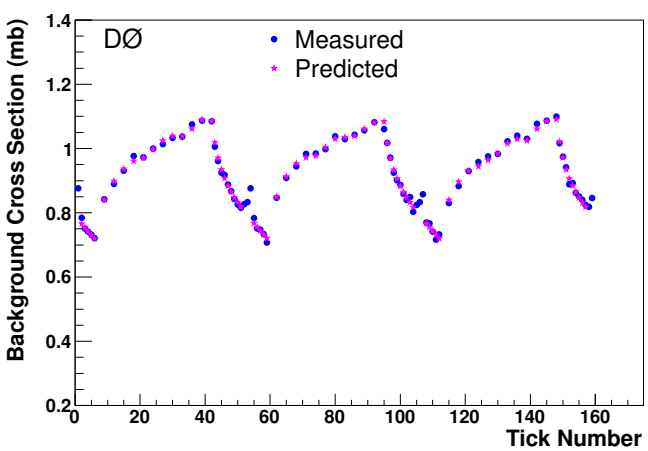

FIG. 22: Comparison of the predicted background cross section and the measured background cross sections.

A model is constructed to describe the observed background cross section. The amplitude of the background produced by a given beam bunch is taken to be proportional to the luminosity for that bunch. It is assumed that the contribution to the background cross section falls exponentially in time following the bunch. There appears to be both a short and long time components in the background, thus a double exponential is used to fit the background. For a bunch occurring at $t = 0$ with luminosity L, the background model predicts that the contribution of the background to future crossings will be

$$\sigma_{BG}(t) = L\left(A_1 e^{-t/\tau_1} + A_2 e^{-t/\tau_2}\right), \qquad \text{(B10)}$$

where A_1 and A_2 are the amplitudes of the two background components and τ_1 and τ_2 are the associated time constants. The background cross sections are fitted using this model. As shown in Fig. 22, this four parameter, two-component model provides a good description of the data. In this particular example, the gap region shows an anomalous up-tick in the background cross section that is likely due to residual beam in these ticks. In fitting the background model, the three ticks with more prominent anomalies have been excluded from the fit as well as the two preceding ticks.

Since this model describes adequately the tick dependence of the background cross section, it is also used to estimate the background cross section during the beam crossings (see Fig. 23). The background cross section varies over time, thus the final background cross section estimate is based on the average over the 35 data samples used for this study. Previously (see Sec. B 2), a background cross section of $\sigma_{BG} = 0.85$ mb was estimated by averaging the individual measurements for north and south monitors, before and after beam crossings. Correcting this value according to the model described above, a background cross section of $\sigma_{BG} = 0.9 \pm 0.1$ mb is calculated, where the uncertainty quoted is the RMS spread.

Appendix C: Background Subtraction

The analytical method used to disentangle the background contribution from the measured multiplicity distributions is described below.

1. Signal and Background Convolution

Given i counters with hits in one of the LM arrays, limits can be placed on the number of signal and background hits even though the same configuration of hits can be

obtained from different combinations of signal and background hits. If l counters have signal hits and p counters have background hits, l and p will be constrained by $l \leq i$, $p \leq i$, and $l + p \geq i$. The last constraint is not an equality because there can be counters with both signal and background hits in them as multiple particles hitting a given counter are counted as a single hit.

The probability of having i counters with hits can be constructed if the multiplicity distributions for signal and background are known. If S_l and B_p are the signal and background probabilities, then the probability d_{ilp} for having i observed counters with hits is given by

$$d_{ilp} = S_l B_p f_{lpi}, \tag{C1}$$

where f_{lpi} is a combinatoric factor that gives the probability that l counters with signal hits and p counters with background hits will yield i counters with observed hits. The combinatoric factor f_{lpi} is derived in Section C 2.

The total probability D_i for observing i hits is obtained by summing over the possible values of l and p:

$$D_i = \sum_{l=0}^{l \leq i} \sum_{p=0}^{p \leq i} S_i B_p f_{lpi} \Theta\left(l + p - i\right), \tag{C2}$$

where the constraints are explicitly represented through the summation limits and the use of the Heaviside step function Θ:

$$\Theta\left(l + p - i\right) = \begin{cases} 1 & \text{for } l + p \geq i, \\ 0 & \text{for } l + p < i. \end{cases} \tag{C3}$$

Similarly, the probability D_{ij} of having i north counters and j south counters with observed hits is given by

$$D_{ij} = \sum_{\substack{l=0 \\ m=0}}^{\substack{l \leq i \\ m \leq j}} \sum_{\substack{p=0 \\ q=0}}^{\substack{p \leq i \\ q \leq j}} S_{lm} B_{pq} f_{lpi} f_{mqj} \Theta\left(l + p - i\right) \Theta\left(m + q - j\right), \tag{C4}$$

where S_{lm} is the probability for having l north counters and m south counters with signal hits and B_{pq} is the probability for having p north counters and q south counters with background hits.

2. Derivation of Combinatoric Factor f_{lpi}

The combinatoric factor f_{lpi} gives the probability for observing i counters with hits given l counters with signal hits and p counters with background hits. The procedure described is based on two assumptions:

1. Background hits are uncorrelated with signal hits. The background hits originate from interactions in earlier beam crossings, while the signal hits originate from interactions in the current beam crossings, making this a reasonable assumption.
2. The counters are either hit or not hit, ignoring the possibility that small amounts of charge from signal and background that are separately below threshold combine to exceed the discriminator threshold to form a hit. The same assumption is also made in the luminosity calculation and has been tested by comparing the north – south coincidence rate in a large sample of 10^8 simulated beam crossings with and without this assumption. No statistically significant difference was found.

If u is the number of counters with both signal and background hits and ν is the number of counters with only background hits, we obtain

$$\begin{aligned} u &= l + p - i, \\ \nu &= i - l. \end{aligned} \tag{C5}$$

The number of ways to arrange u hits with both signal and background among l counters with signal hits is given by

$$\binom{l}{u} = \frac{l!}{u!\,(l-u)!} = \frac{l!}{(l+p-i)!\,(i-p)!}. \tag{C6}$$

Similarly, the number of ways that ν background-only hits can be distributed among the $N - l$ counters without signal hits is

$$\binom{N-l}{\nu} = \frac{(N-l)!}{\nu!\,(N-l-\nu)!} = \frac{(N-l)!}{(i-l)!\,(N-i)!}. \tag{C7}$$

Thus, the total number of background hit combinations is the product of Eqs. C6 and C7

$$\binom{l}{u}\binom{N-l}{\nu} = \frac{l!\,(N-l)!}{(l+p-i)!\,(i-p)!\,(i-l)!\,(N-i)!}\ . \tag{C8}$$

The total number of ways to arrange p background hits among N counters is

$$\binom{N}{p} = \frac{N!}{p!\,(N-p)!}\ . \tag{C9}$$

Each arrangement of background hits among the N counters is assumed to be equally likely, therefore the probability of having i counters with hits, given l counters with signal hits and p counters with background hits, is the number of arrangements meeting this condition divided by the total number of arrangements of the background hits:

$$\begin{aligned} f_{lpi} &= \frac{\binom{l}{u}\binom{N-l}{\nu}}{\binom{N}{p}} \\ &= \frac{l!\,(N-l)!p!\,(N-p)!}{(l+p-i)!\,(i-p)!\,(i-l)!\,(N-i)!N!}\ . \end{aligned} \tag{C10}$$

While the derivation did not treat signal and background hits symmetrically, the final result includes the expected $l \leftrightarrow p$ symmetry.

3. Unfolding Procedure

Once the data and background multiplicity distributions are measured, an unfolding procedure is used to extract the signal multiplicity distribution. To simplify the notation, the 2D multiplicity distributions, with indexes ranging from 0 to 24, are re-labeled to use a single index that ranges from 0 to 624. For example, the 2D multiplicity distributions for counters with observed hits can be written as:

$$\begin{aligned} D_\alpha &\equiv D_{ij} \quad \text{where} \quad \alpha = 25i + j \\ S_\beta &\equiv S_{lm} \quad \text{where} \quad \beta = 25l + m \\ B_\gamma &\equiv B_{pq} \quad \text{where} \quad \gamma = 25p + q. \end{aligned} \tag{C11}$$

The tensor $T_{\alpha\beta\gamma}$ is defined as follows:

$$T_{\alpha\beta\gamma} = \begin{cases} f_{lpi} f_{jmq} & \text{for} \begin{array}{l} l \le i, p \le i, m \le j, q \le j, \\ i \le l + p, j \le m + q \end{array} \\ 0 & \text{otherwise.} \end{cases} \tag{C12}$$

In this notation, Eq. C4 for the convolution of signal and background multiplicity distributions can be written as

$$D_\alpha = T_{\alpha\beta\gamma} S_\beta B_\gamma, \tag{C13}$$

where the convention of implied summation for repeated indices has been used. To solve for the signal multiplicity distribution in this notation, the folding and unfolding matrices F and U are defined:

$$F_{\alpha\beta} = T_{\alpha\beta\gamma} B_\gamma \tag{C14}$$

$$U = F^{-1}. \tag{C15}$$

Substituting these matrices into Eq. C13 the following matrix equations are extracted:

$$D = FS \tag{C16}$$

$$S = F^{-1} D = UD \tag{C17}$$

Thus, the signal multiplicity distribution is obtained by taking the product of the unfolding and data matrices. The inversion of the folding matrix F is only necessary for a simultaneous determination of the covariance matrix for the signal multiplicity distribution. Otherwise a linear equation solver can be used to find the signal multiplicity distribution S.

4. Covariance Matrix for the Signal Multiplicity Distribution

The unfolding procedure introduces correlations among the multiplicity bins, so that the uncertainty is represented by a 625×625 element covariance matrix. Standard error propagation techniques are used to determine the covariance matrix for the unfolded signal multiplicity distribution,

$$(\delta D)_\alpha = T_{\alpha\beta\gamma} (\delta S)_\beta B_\gamma + T_{\alpha\beta\gamma} S_\beta (\delta B)_\gamma . \tag{C18}$$

This result can be formulated as a matrix equation:

$$G_{\alpha\gamma} = T_{\alpha\beta\gamma} S_\beta \tag{C19}$$

$$\delta D = F(\delta S) + G(\delta B) \tag{C20}$$

$$\begin{aligned} \delta S &= F^{-1} [(\delta D) - G(\delta B)] \\ &= U [(\delta D) - G(\delta B)] . \end{aligned} \tag{C21}$$

The covariance matrix for the multiplicity distribution of counters with signal hits is given by:

$$\begin{aligned} C^S &\equiv \left\langle (\delta S)(\delta S)^T \right\rangle \\ &= \left\langle U [(\delta D) - G(\delta B)] [(\delta D) - G(\delta B)]^T U^T \right\rangle . \end{aligned} \tag{C22}$$

Since the observed signal + background multiplicity distribution is uncorrelated with the background multiplicity distribution:

$$\begin{aligned} C^S &= U \left\langle (\delta D)(\delta D)^T \right\rangle U^T + UG \left\langle (\delta B)(\delta B)^T \right\rangle G^T U^T \\ &= UC^D U^T + UGC^B G^T U^T, \end{aligned} \tag{C23}$$

where C^D and C^B are the covariance matrices for the data and background multiplicity distributions. The data and background covariance matrices simply contain diagonal binomial error terms:

$$C^D_{\alpha\beta} = \delta_{\alpha\beta} D_\alpha (1 - D_\alpha) / N_D \tag{C24}$$

$$C^B_{\alpha\beta} = \delta_{\alpha\beta} B_\alpha (1 - B_\alpha) / N_B \tag{C25}$$

where $\delta_{\alpha\beta}$ is the Kronecker δ function and N_D and N_B are the total number of entries in the data and background multiplicity distributions, respectively.